

University of Groningen

Predicting Drug Concentration-Time Profiles in Multiple CNS Compartments Using a Comprehensive Physiologically-Based Pharmacokinetic Model

Yamamoto, Yumi; Väitalo, Pyry A; Huntjens, Dymphy R; Proost, Johannes H; Vermeulen, An; Krauwinkel, Walter; Beukers, Margot W; van den Berg, Dirk-Jan; Hartman, Robin; Wong, Yin Cheong

Published in:

CPT: Pharmacometrics & Systems Pharmacology

DOI:

[10.1002/psp4.12250](https://doi.org/10.1002/psp4.12250)

IMPORTANT NOTE: You are advised to consult the publisher's version (publisher's PDF) if you wish to cite from it. Please check the document version below.

Document Version

Publisher's PDF, also known as Version of record

Publication date:

2017

[Link to publication in University of Groningen/UMCG research database](#)

Citation for published version (APA):

Yamamoto, Y., Väitalo, P. A., Huntjens, D. R., Proost, J. H., Vermeulen, A., Krauwinkel, W., Beukers, M. W., van den Berg, D-J., Hartman, R., Wong, Y. C., Danhof, M., van Hasselt, J. G. C., & de Lange, E. C. M. (2017). Predicting Drug Concentration-Time Profiles in Multiple CNS Compartments Using a Comprehensive Physiologically-Based Pharmacokinetic Model. *CPT: Pharmacometrics & Systems Pharmacology*, 6(11), 765-777. <https://doi.org/10.1002/psp4.12250>

Copyright

Other than for strictly personal use, it is not permitted to download or to forward/distribute the text or part of it without the consent of the author(s) and/or copyright holder(s), unless the work is under an open content license (like Creative Commons).


The publication may also be distributed here under the terms of Article 25fa of the Dutch Copyright Act, indicated by the "Taverne" license. More information can be found on the University of Groningen website: <https://www.rug.nl/library/open-access/self-archiving-pure/taverne-amendment>.

Take-down policy

If you believe that this document breaches copyright please contact us providing details, and we will remove access to the work immediately and investigate your claim.

ORIGINAL ARTICLE

Predicting Drug Concentration-Time Profiles in Multiple CNS Compartments Using a Comprehensive Physiologically-Based Pharmacokinetic Model

Yumi Yamamoto¹, Pyry A. Väitalo¹, Dymphy R. Huntjens², Johannes H. Proost³, An Vermeulen², Walter Krauwinkel⁴, Margot W. Beukers⁵, Dirk-Jan van den Berg¹, Robin Hartman¹, Yin Cheong Wong ¹, Meindert Danhof¹, John G. C. van Hasselt¹ and Elizabeth C. M. de Lange^{1*}

Drug development targeting the central nervous system (CNS) is challenging due to poor predictability of drug concentrations in various CNS compartments. We developed a generic physiologically based pharmacokinetic (PBPK) model for prediction of drug concentrations in physiologically relevant CNS compartments. System-specific and drug-specific model parameters were derived from literature and *in silico* predictions. The model was validated using detailed concentration-time profiles from 10 drugs in rat plasma, brain extracellular fluid, 2 cerebrospinal fluid sites, and total brain tissue. These drugs, all small molecules, were selected to cover a wide range of physicochemical properties. The concentration-time profiles for these drugs were adequately predicted across the CNS compartments (symmetric mean absolute percentage error for the model prediction was <91%). In conclusion, the developed PBPK model can be used to predict temporal concentration profiles of drugs in multiple relevant CNS compartments, which we consider valuable information for efficient CNS drug development.

CPT Pharmacometrics Syst. Pharmacol. (2017) 6, 765–777; doi:10.1002/psp4.12250; published online 11 September 2017.

Study Highlights

WHAT IS THE CURRENT KNOWLEDGE ON THE TOPIC?

❑ Lack of knowledge of the target-site concentrations in the CNS is a major hurdle in the development of new CNS drugs.

WHAT QUESTION DID THIS STUDY ADDRESS?

❑ A generic PBPK model in the rat CNS was proposed.

WHAT THIS STUDY ADDS TO OUR KNOWLEDGE

❑ The developed PBPK model was able to predict time-dependent concentration profiles of many drugs

with distinctively different physicochemical properties in multiple physiologically relevant compartments in the CNS.

HOW MIGHT THIS CHANGE DRUG DISCOVERY, DEVELOPMENT, AND/OR THERAPEUTICS?

❑ The developed model structure can be used to predict concentration-time profiles in rats and offers a scientific basis for the development of CNS drugs, in principle, without the need of using animals.

The development of drugs targeting diseases of the central nervous system (CNS) represents one of the most significant challenges in the research of new medicines.¹ Characterization of exposure-response relationships at the drug target site may be of critical importance to reduce attrition. However, unlike for many other drugs, prediction of target-site concentrations for CNS drugs is complex, among other factors, due to the presence of the blood-brain barrier (BBB) and the blood-cerebrospinal fluid barrier (BCSFB). Moreover, direct measurement of human brain concentrations is highly restricted for ethical reasons. Therefore, new approaches that can robustly predict human brain concentrations of novel drug candidates based on *in vitro* and *in silico* studies are of great importance.

Several pharmacokinetic (PK) models to predict CNS exposure have been published with different levels of complexity.² The majority of these models depend on animal data. Furthermore, these models have typically not been validated against human CNS drug concentrations.² We previously published a general multicompartmental CNS PK model structure, which was developed using PK data obtained from rats.

Quantitative structure-property relationship (QSPR) models can be used to predict drug BBB permeability and $K_{p,uu,brain_{ECF}}$ (unbound brain extracellular fluid-to-plasma concentration ratio)^{3–5} without performing novel experiments, but these QSPR models have not taken into account the time course of CNS distribution. Therefore, there exists an unmet need for approaches to predict drug

¹Division of Pharmacology, Cluster Systems Pharmacology, Leiden Academic Centre for Drug Research, Leiden University, Leiden, The Netherlands; ²Quantitative Sciences, Janssen Research and Development, a division of Janssen Pharmaceutica NV, Beerse, Belgium; ³Division of Pharmacokinetics, Toxicology and Targeting, University of Groningen, Groningen, The Netherlands; ⁴Department of Clinical Pharmacology and Exploratory Development, Astellas Pharma BV, Leiden, The Netherlands; ⁵Science Business Support, Leiden, the Netherlands. *Correspondence: E C M de Lange (ecmdelange@lacdr.leidenuniv.nl)

Received 3 April 2017; accepted 28 August 2017; published online on 11 September 2017. doi:10.1002/psp4.12250

This article was published online on 13 October 2017. An error was subsequently identified in the author line. This notice is included in the online version to indicate this version has been corrected 27 October 2017.

target-site concentration-time profiles without the need of *in vivo* animal experiments.

Physiologically based pharmacokinetic (PBPK) modeling represents a promising approach for the prediction of CNS drug concentrations. Previously, such models have been widely used to predict tissue concentrations.⁶ The PBPK models typically distinguish between drug-specific and system-specific parameters, therefore, enabling predictions across drugs and species. However, PBPK models for the CNS have been of limited utility due to a lack of relevant physiological details for mechanism of transport across the BBB and BCSFB, and for drug distribution within the CNS.²

Capturing the physiological compartments, flows, and transport processes in a CNS PBPK model is critically important to predict PK profiles in the CNS. The CNS comprises of multiple key physiological compartments,² including brain extracellular fluid (brain_{ECF}), brain intracellular fluid (brain_{ICF}), and multiple cerebrospinal fluid (CSF) compartments. The brain_{ECF} and brain_{ICF} compartments are considered highly relevant target sites for CNS drugs, whereas CSF compartments are often used to measure CNS-associated drug concentrations, if brain_{ECF} and brain_{ICF} information cannot be obtained. Furthermore, cerebral blood flow (CBF) and physiological flows within the CNS, such as the brain_{ECF} flow and CSF flows, influence drug distribution across CNS compartments. Next to binding to protein and lipids, pH-dependent distribution in subcellular compartments, such as trapping of basic compounds in lysosomes, needs to be considered. With regard to the transfer processes across the BBB and BCSFB, passive diffusion via the paracellular and transcellular pathways and active transport by influx and/or efflux transporters need to be addressed.

At both BBB and BCSFB barriers, the cells are interconnected by tight junctions, which limit drug exchange via the paracellular pathway.⁷ Paracellular and transcellular diffusion depend on the aqueous diffusivity coefficient and membrane permeability of the compound, which can be related to the physicochemical properties. The combination of these transport routes may differ between individual drugs, which complicate the prediction of plasma-brain transport.

System-specific information on physiological parameters can be used in scaling between species. Many of these system-specific parameters can or have been obtained from *in vitro* and *in vivo* experiments. Drug-specific parameters can be derived by *in vitro* and QSPR approaches, and can be used for the scaling between drugs. A comprehensive CNS PBPK model can integrate system-specific and drug-specific parameters to potentially enable the prediction of the brain distribution of drugs without the need to conduct *in vivo* animal studies.

The purpose of the current work is to develop a comprehensive PBPK model to predict drug concentration-time profiles in the multiple physiologically relevant compartments in the CNS, based on system-specific and drug-specific parameters without the need to generate *in vivo* data. We specifically consider the prediction of PK profiles in the CNS during pathological conditions, which may have distinct effects on paracellular diffusion, transcellular

diffusion, and active transport. Therefore, we include a range of such transport mechanisms in our CNS PBPK model. This model is evaluated using previously published detailed multilevel brain and CSF concentration-time data for 10 drugs with highly diverse physicochemical properties.

MATERIALS AND METHODS

We first empirically modeled plasma PK using available plasma PK data, which was used as the basis for the CNS PBPK model. This CNS model was based entirely on parameters derived from literature and *in silico* predictions. Model development was performed using NONMEM version 7.3.

Empirical plasma PK model

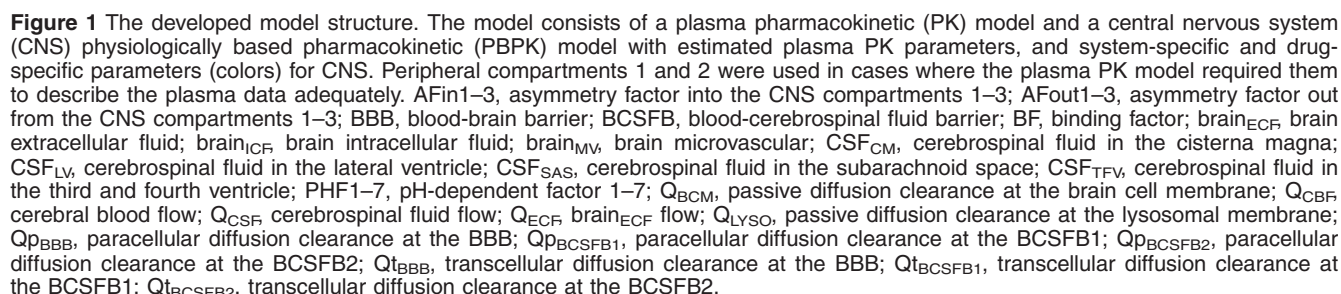
Plasma PK models were systematically developed using *in vivo* data with a mixed-effects modeling approach. One, two, and three-compartment models were evaluated. Inter-individual variability and interstudy variability were incorporated on each PK parameter using exponential models. Proportional and combined additive-proportional residual error models were considered. Model selection was guided by the likelihood ratio test ($P < 0.05$), precision of the parameter estimates, and standard goodness of fit plots.⁸

CNS PBPK model development

A generic PBPK model structure was developed based on the previously published generic multicompartmental CNS distribution model (Figure 1),⁹ which consists of plasma, brain_{ECF}, brain_{ICF}, CSF in the lateral ventricle (CSF_{LV}), CSF in the third and fourth ventricle (CSF_{TFV}), CSF in the cisterna magna (CSF_{CM}), and CSF in the subarachnoid space (CSF_{SAS}) compartments. We added new components: (1) an acidic subcellular compartment representing lysosomes to account for pH-dependent drug distribution; (2) a brain microvascular compartment (brain_{MV}) to account for CBF vs. permeability rate-limited kinetics; and (3) separation of passive diffusion at the BBB and BCSFB into its transcellular and paracellular components.

System-specific parameters

Physiological values of the distribution volumes of all the CNS compartments, flows, surface area (SA) of the BBB (SA_{BBB}), SA of the BCSFB (SA_{BCSFB}), SA of the total brain cell membrane (BCM; SA_{BCM}), and the width of BBB (Width_{BBB}) were collected from literature. The SA_{BCSFB} was divided into SA_{BCSFB1}, which is a surface area around CSF_{LV}, and SA_{BCSFB2}, which is a surface area around CSF_{TFV}. The lysosomal volume was calculated based on the volume ratio of lysosomes to brain intracellular fluid of brain parenchyma cells (1:80),¹⁰ and the SA of the lysosome (SA_{LYSO}) is calculated by obtaining the lysosome number per cell using the lysosomal volume and the diameter of each lysosome.¹¹ Transcellular and paracellular diffusion were separately incorporated into the models, therefore, the ratio of SA_{BBB} and SA_{BCSFB} for transcellular diffusion and paracellular diffusion were required for the calculation. Based on electron microscopic cross-section pictures of brain capillary, the length of a single brain microvascular endothelial cell was estimated to be around 17 μm and the length of the



Active transport. The impact of the net effect of active transporters on the drug exchange at the BBB and BCSFB was incorporated into the model using asymmetry factors (AF_{in1–3} and AF_{out1–3}). The AFs were calculated from K_{p,uu,brain_{ECF}}, K_{p,uu,CSF_{LV}} (unbound CSF_{LV}-to-plasma concentration ratio) and K_{p,uu,CSF_{CM}} (unbound CSF_{CM}-to-plasma concentration ratio), such that they produced the same K_{p,uu} values within the PBPK model at the steady-state. Therefore, the AFs were dependent on both the K_{p,uu} values and the structure and parameters of the PBPK model. If the K_{p,uu} values were larger than 1 (i.e., net active influx), then AF_{in1}, AF_{in2}, and AF_{in3} were derived from K_{p,uu,brain_{ECF}}, K_{p,uu,CSF_{LV}}, and K_{p,uu,CSF_{CM}}, respectively, whereas AF_{out1–3} were fixed to 1. If the K_{p,uu} values were smaller than 1 (i.e., net active efflux), then AF_{out1}, AF_{out2}, and AF_{out3} were derived from K_{p,uu,brain_{ECF}}, K_{p,uu,CSF_{LV}}, and K_{p,uu,CSF_{CM}}, respectively, whereas AF_{in1–3} were fixed to 1. In the

analysis, $K_{p,uu,brain_{ECF}}$, $K_{p,uu,CSF_{LV}}$, and $K_{p,uu,CSF_{CM}}$ were derived from previous *in vivo* animal experiments.⁹ The steady-state differential equations in the PBPK model were solved using the Maxima Computer Algebra System (<http://maxima.sourceforge.net>) to obtain algebraic solutions for calculating AFs from the $K_{p,uu}$ values. The detailed algebraic solutions for each AF are provided in **Supplementary Material S1**.

Combined system-specific and drug-specific parameters

Passive diffusion across the brain barriers. Passive diffusion clearance at the BBB and BCSFB (Q_{BBB} and Q_{BCSFB} , respectively) was obtained from a combination of paracellular and transcellular diffusion, Q_p and Q_t , respectively (Eq. 3).

$$Q_{BBB/BCSFB} (mL/min) = Q_{pBBB/BCSFB} + Q_{tBBB/BCSFB} \quad (3)$$

where $Q_{BBB/BCSFB}$ represents the passive diffusion clearance at the BBB/BCSFB, $Q_{pBBB/BCSFB}$ represents the paracellular diffusion clearance at the BBB/BCSFB, and $Q_{tBBB/BCSFB}$ represents the transcellular diffusion clearance at the BBB/BCSFB.

The paracellular diffusion clearance was calculated with the aqueous diffusivity coefficient (Daq), $Width_{BBB/BCSFB}$, and SA_{BBBp} or SA_{BCSFBp} using Eq. 4.

$$Q_{pBBB/BCSFB} (mL/min) = \frac{Daq}{Width_{BBB/BCSFB}} \times SA_{BBBp/BCSFBp} \quad (4)$$

The transcellular diffusion clearance was calculated with the transmembrane permeability and SA_{BBBt} or SA_{BCSFBt} using Eq. 5.

$$Q_{tBBB/BCSFB} (mL/min) = \frac{1}{2} * P_0^{transcellular} \times SA_{BBBt/BCSFBt} \quad (5)$$

where the factor 1/2 is the correction factor for passage over two membranes instead of one membrane in the transcellular passage.

Active transport across the brain barriers. To take into account the net effect of the active transporters at the BBB and BCSFB, AFs were added on $Q_{tBBB/BCSFB}$ (Eqs. 6 and 7).

$$Q_{BBB/BCSFB_in} (mL/min) = Q_{pBBB/BCSFB} + Q_{tBBB/BCSFB} * AF_{in} \quad (6)$$

$$Q_{BBB/BCSFB_out_withoutPHF} (mL/min) = Q_{pBBB/BCSFB} + Q_{tBBB/BCSFB} * AF_{out} \quad (7)$$

where $Q_{BBB/BCSFB_in}$ represents the drug transport clearance from $brain_{MV}$ to $brain_{ECF}/CSFs$, and $Q_{BBB/BCSFB_out_withoutPHF}$ represents the drug transport clearance from $brain_{ECF}/CSFs$ to $brain_{MV}$ without taking into account the pH-dependent kinetics (to be taken into account separately; see below).

Cellular and subcellular distribution. Passive diffusion at the BCM (Q_{BCM}) and at the lysosomal membrane (Q_{LYSO}) was

described with the transmembrane permeability together with SA_{BCM} or SA_{LYSO} , respectively (Eqs. 8 and 9).

$$Q_{BCM} (mL/min) = P_0^{transcellular} \times SA_{BCM} \quad (8)$$

$$Q_{LYSO} (mL/min) = P_0^{transcellular} \times SA_{LYSO} \quad (9)$$

where Q_{BCM} represents the passive diffusion clearance at the BCM, and Q_{LYSO} represents the passive diffusion clearance at the lysosomal membrane.

pH-dependent partitioning. We considered the differences in pH in plasma (pH 7.4) and in relevant CNS compartments, namely $brain_{ECF}$ (pH_{ECF} 7.3), CSF (pH_{CSF} 7.3), $brain_{ICF}$ (pH_{ICF} 7.0), and lysosomes (pH_{LYSO} 5.0).¹⁸ The impact of pH differences on the passive diffusion clearance from $brain_{ECF}$ to $brain_{MV}$ (PHF1), from CSF_{LV} to $brain_{MV}$ (PHF2), from CSF_{TFV} to $brain_{MV}$ (PHF3), from $brain_{ECF}$ to $brain_{ICF}$ (PHF4), from $brain_{ICF}$ to $brain_{ECF}$ (PHF5), from $brain_{ICF}$ to lysosomes (PHF6), and from lysosomes to $brain_{ICF}$ (PHF7) were described by pH-dependent factors, which were defined as the ratio of the unionized fraction of each compound at the pH in a particular compartment and the unionized fraction in plasma. The PHFs were calculated from the pK_a of each compound and the pH of a particular compartment. The equations are developed using the classical Henderson-Hasselbalch equation,^{19,20} and are based on the assumption that there is no active transport.

$$PHF_{base1} = PHF_{base4} = \frac{10^{pK_a - 7.4} + 1}{10^{pK_a - pH_{ECF}} + 1} \quad (10)$$

$$PHF_{base2} = PHF_{base3} = \frac{10^{pK_a - 7.4} + 1}{10^{pK_a - pH_{CSF}} + 1} \quad (11)$$

$$PHF_{base5} = PHF_{base6} = \frac{10^{pK_a - 7.4} + 1}{10^{pK_a - pH_{ICF}} + 1} \quad (12)$$

$$PHF_{base7} = \frac{10^{pK_a - 7.4} + 1}{10^{pK_a - pH_{LYSO}} + 1} \quad (13)$$

$$PHF_{acid1} = PHF_{acid4} = \frac{10^{7.4 - pK_a} + 1}{10^{pH_{ECF} - pK_a} + 1} \quad (14)$$

$$PHF_{acid2} = PHF_{acid3} = \frac{10^{7.4 - pK_a} + 1}{10^{pH_{CSF} - pK_a} + 1} \quad (15)$$

$$PHF_{acid5} = PHF_{acid6} = \frac{10^{7.4 - pK_a} + 1}{10^{pH_{ICF} - pK_a} + 1} \quad (16)$$

$$PHF_{acid7} = \frac{10^{7.4 - pK_a} + 1}{10^{pH_{LYSO} - pK_a} + 1} \quad (17)$$

where $PHF_{base1-7}$ are PHF1-7 for basic compounds, $PHF_{acid1-7}$ are PHF1-7 for acidic compounds, and 7.4 is the pH in the plasma compartment.

The impact of pH differences on the drug distribution among $brain_{ECF}$, CSF, $brain_{ICF}$ and lysosomes was added on Q_{BCM} and Q_{LYSO} using PHFs with the following Eqs. 18–24 based on the assumption that the transport clearance is proportional to the unionized fraction of each compound.

$$Q_{BBB_out} (mL/min) = Q_{BBB_out_withoutPHF} \times PHF1 \quad (18)$$

$$Q_{BCSFB1_out} (mL/min) = Q_{BCSFB_withoutPHF} \times PHF2 \quad (19)$$

$$Q_{BCSFB2_out} (mL/min) = Q_{BCSFB_withoutPHF} \times PHF3 \quad (20)$$

$$Q_{BCM_in} (mL/min) = Q_{BCM} \times PHF4 \quad (21)$$

$$Q_{BCM_out} (mL/min) = Q_{BCM} \times PHF5 \quad (22)$$

$$Q_{LYSO_in} (mL/min) = Q_{LYSO} \times PHF6 \quad (23)$$

$$Q_{LYSO_out} (mL/min) = Q_{LYSO} \times PHF7 \quad (24)$$

where Q_{BBB_out} represents the drug transport clearance from $brain_{ECF}$ to $brain_{MV}$, Q_{BCSFB1_out} represents the drug transport clearance from CSF_{LV} to $brain_{MV}$, Q_{BCSFB2_out} represents the drug transport clearance from CSF_{TFV} to $brain_{MV}$, Q_{BCM_in} represents the drug transport clearance from $brain_{ECF}$ to $brain_{ICF}$ and Q_{BCM_out} represents the drug transport clearance from $brain_{ICF}$ to $brain_{ECF}$. The Q_{LYSO_in} represents the drug transport clearance from $brain_{ICF}$ to lysosomes, and Q_{BCM_out} represents the drug transport clearance from lysosomes to $brain_{ICF}$.

Drug binding. Drug binding to brain tissue components was taken into account in the model using a binding factor (BF) under the assumption that drug binding to the tissue happens instantly. The BF was calculated from Kp (total brain-to-plasma concentration ratio) by solving the BF that results in the same Kp value in the model, using the Maxima program, as described above (**Supplementary Material S1**). The Kp for each compound was calculated using the compounds' log P, the composition of brain tissue and plasma, free fraction in plasma ($f_{u,p}$) and free fraction in brain ($f_{u,b}$) with the following equation²¹:

$$Kp = \frac{[10^{\log P} \times (Vnlb + 0.3 \times Vphb) + 0.7 \times Vphb + Vwb / f_{u,b}]}{[10^{\log P} \times (Vnlp + 0.3 \times Vphp) + 0.7 \times Vphp + Vwp / f_{u,p}]} \quad (25)$$

where $Vnlb$, $Vphb$, Vwb , $Vnlp$, $Vphp$, and Vwp represent the rat volume fractions of brain neutral lipids (0.0392), brain phospholipids (0.0533), brain water (0.788), plasma neutral lipids (0.00147), plasma phospholipids (0.00083), and plasma water (0.96), respectively.²²

In vivo data collection for model evaluation

In vivo data obtained from multiple brain locations were used to evaluate the developed model.^{9,23–29} An overview of experimental design and data for 10 compounds with substantially different physicochemical characteristics is provided in **Table 1**.^{9,23–29} All data were previously published, except the remoxipride total brain tissue data. General animal surgery procedures, experimental protocol, and bioanalytical methods for remoxipride total brain tissue data are described in **Supplementary Material S2**, and experimental protocol details for each drug are summarized in **Supplementary Table S1**.

Evaluation of the PBPK model

The PBPK model performance was evaluated by the comparison of model predictions with the concentration-time profiles in $brain_{ECF}$, CSF_{LV} , CSF_{CM} , and total brain tissue of

Table 1 Summary of rat multilevel brain and CSFs data for model evaluation

Table 1 Summary of rat midline/ventral brain and CSF's data for inductor evaluation												
	Acetaminophen	Atenolol	Methotrexate	Morphine	Morphine	Paliperidone	Phenytoin	Quinidine	Raclopride	Remoxipride	Remoxipride	Risperidone
Study design												
No. of animals	16	5	23	65	18	21	14	41	19	29	65	16
Dosage, mg/kg (infusion time, min)	15 (10)	10 (1)	40, 80 (10)	4, 10, 40 (10)	10, 40 (10)	0.5 (20)	20, 30, 40 (10)	10, 20 (10)	0.56 (10)	4, 8, 16 (30)	0.7, 5.2, 14 (10)	2 (20)
Data												
Plasma	X	X	X	X	X	X	X	X	X	X	X	X
Brain _{ECF}	X	X	X	X	X	X	X	X	X	X	X	X
CSF _{LV}	X		X					X			X	
CSF _{CM}	X		X			X		X			X	
Total brain tissue										X (new data)	X (new data)	
References	24	25	23	26	27	9	9	28	X	30 (except total brain tissue data)	9 (except total brain tissue data)	9

$Brain_{ECF}$, brain extracellular fluid compartment; CSF_{LV} , cerebrospinal fluid compartment in the lateral ventricle; CSF_{CM} , cerebrospinal fluid compartment in the cisterna magna.

10 compounds. We performed 200 simulations for each compound, including random effect estimates for the plasma PK model. Based on these, we calculated the prediction error (PE) and symmetric mean absolute percentage error (SMAPE), see Eqs. 26 and 27.

$$PE = \frac{Y_{OBS,ij} - Y_{PRED,ij}}{(Y_{OBS,ij} + Y_{PRED,ij})/2} \quad (26)$$

$$SMAPE = \frac{1}{N} \sum_{k=1}^N |PE| \times 100 \quad (27)$$

where $Y_{OBS,ij}$ is the j th observation of the i th subject, $Y_{PRED,ij}$ is the j th mean prediction of the i th subject, and N is the number of observations.

RESULTS

Plasma PK model

The estimated parameters for the descriptive plasma PK models were obtained with good precision and summarized in **Table 2**. The models describe plasma concentration-time profiles very well for all compounds except risperidone (**Supplementary Figure S1**). For remoxipride, a small underprediction was observed at later time points.

CNS PBPK model

The NONMEM model codes for the 10 compounds are provided in **Supplementary Material S3–S13**. The values of the system-specific and drug-specific parameters are summarized in **Tables 3**^{30–44} and **4**, respectively. The combined system-specific and drug-specific parameters are summarized in **Table 5**. Overall, the developed generic PBPK model could adequately predict the rat data in brain_{ECF}, CSF_{LV}, CSF_{CM}, and total brain tissue. **Figure 2** shows the PE for each compound and each CNS compartment. The PE for risperidone brain_{ECF} and CSF_{CM} showed modest underprediction. For the other drugs, the PEs were distributed within two standard deviations and no specific trends were observed across time, compounds, and CNS locations. The SMAPEs for the model prediction in brain_{ECF}, CSF_{LV}, CSF_{CM}, and total brain tissue were 72%, 71%, 69%, and 91%, respectively, indicating that the model could predict concentration-time profiles in these compartments with less than twofold prediction error. The concentration-time plots of individual predictions vs. observations across drugs and dose levels are provided (**Supplementary Figure S1**).

Impact of cerebral blood flow

Cerebral blood flow (Q_{CBF}) is 1.2 mL/min.⁴⁴ Therefore, for strong lipophilic compounds, for instance, quinidine, the drug transport clearance from plasma to the brain_{ECF} (BBB permeability) is limited by Q_{CBF} because $Q_{BBB,in}$ and $Q_{BBB,out}$ of quinidine were 9.1 and 5.1 mL/min, respectively (**Tables 3 and 5**).

Impact of distinct paracellular and transcellular pathways on total diffusion at the BBB, and BCSFB (Q_{BBB} , Q_{BCSFB1} , and Q_{BCSFB2})

The Q_{BBB} , Q_{BCSFB1} , and Q_{BCSFB2} were determined by the combination of paracellular and transcellular diffusion in the

model. Even though the SA_{BBBp} is very small compared to the SA_{BBBt} (0.006: 99.8), paracellular diffusion had an impact on the values of Q_{BBB} , Q_{BCSFB1} , and Q_{BCSFB2} especially for hydrophilic compounds. For instance, the values of transcellular diffusion (Q_{tBBB}) and paracellular diffusion (Q_{pBBB}) for methotrexate, which is the most hydrophilic compound in this study, were 0.000080 and 0.087 mL/min, respectively (**Table 5**). Thus, the Q_{BBB} of methotrexate was determined mainly by paracellular diffusion. For quinidine, which is the most lipophilic compound in the study, the Q_{BBB} was mainly determined by CBF limited transcellular diffusion (Q_{tBBB} and Q_{pBBB} were 7.6 and 0.10 mL/min, respectively).

Rate limiting drug transport clearance for intra-extracellular exchange ($Q_{BCM,in}$ and $Q_{BCM,out}$)

The $Q_{BCM,in}$ and $Q_{BCM,out}$ were higher than $Q_{BBB,in}$ and $Q_{BBB,out}$ for acetaminophen, paliperidone, phenytoin, quinidine, raclopride, remoxipride, and risperidone. The $Q_{BCM,in}$ and $Q_{BCM,out}$ are lower than $Q_{BBB,in}$ and $Q_{BBB,out}$ for methotrexate (**Table 5**). This suggests that the transport clearance from brain_{MV}, via brain_{ECF}, to brain_{ICF} is limited by $Q_{BBB,in}$ and $Q_{BBB,out}$ for acetaminophen, paliperidone, phenytoin, quinidine, raclopride, remoxipride, and risperidone, whereas it is limited by $Q_{BCM,in}$ and $Q_{BCM,out}$ for methotrexate.

Surface area of BCSFB to determine the paracellular and transcellular diffusion clearance around CSF_{LV} and CSF_{TFV}

In our model, we assumed that the SA of the BCSFB around CSF_{LV} (SA_{BCSFB1}) and CSF_{TFV} (SA_{BCSFB2}) are equal in size (50% of the total SA_{BCSFB} for each). The SA is one of the key factors that determine the paracellular and transcellular diffusion clearance across the BCSFB1 and BCSFB2. However, the early-time predictions for CSF_{LV} for acetaminophen, quinidine, and remoxipride indicate an overprediction of the paracellular and transcellular diffusion clearance (**Figure 2 and Supplementary Figure S1**), suggesting that the SA of BCSFB1 is <50% of the total SA_{BCSFB} .

Impact of active transporters to determine the extent of drug exposure in the CNS compartments

Active transporters govern the extent of drug exposure in the brain and CSFs. For most of the compounds, the impact of active transporters among $K_{p,uu,brain_{ECF}}$, $K_{p,uu,CSF_{LV}}$, and $K_{p,uu,CSF_{CM}}$ was assumed to be identical, except for methotrexate. Different $K_{p,uu,CSF_{LV}}$ (0.0066) and $K_{p,uu,CSF_{CM}}$ (0.0024) were observed for methotrexate, which were taken into account in the PBPK model by asymmetry factors AFout2 and AFout3. The extent of drug entry into the brain and CSF was predicted well for all compounds, except for morphine at the 4 mg/kg dose (**Supplementary Figure S1**).

DISCUSSION

The developed CNS PBPK model resulted in adequate predictions of concentration-time courses for 10 diverse drugs

Table 2 Parameter estimates for plasma pharmacokinetics of the 10 compounds

		Parameter estimates (RSE, %)									
		Acetaminophen	Atenolol	Methotrexate	Morphine	Paliperidone	Phenytoin	Quinidine	Raclopride	Remoxipride	Risperidone
CL _{PL}	mL/min	15.8 (9.10)	7.13 (20.6)	8.04 (15.9)	22.6 (7.70)	196 (13.0)	36.0 (8.90)	162 (4.10)	46.4 (4.30)	42.2 (4.90)	886 (33.2)
Q _{PL_PER1}	mL/min	33.8 (33.7)	NA	28.5 (30.7)	30.8 (10.0)	61.5 (86.2)	265 (12.7)	829 (6.80)	13.4 (27.5)	33.8 (20.7)	NA
Q _{PL_PER2}	mL/min	NA	NA	3.33 (34.8)	7.21 (10.2)	NA	NA	NA	69.2 (7.50)	14.0 (10.1)	NA
V _{PL}	mL	49.5 (59.0)	256 (27.0)	28.0 (55.0)	152 (11.1)	26,400 (12.6)	943 (21.5)	670 (13.3)	48.9 (16.3)	83.7 (18.3)	43,100 (28.1)
V _{PER1}	mL	363 (33.1)	NA	111 (14.6)	530 (9.10)	3,580 (35.8)	2,050 (7.50)	11,300 (3.20)	684 (19.2)	253 (10.9)	NA
V _{PER2}	mL	NA	NA	83.5 (34.9)	1,200 (10.8)	NA	NA	NA	493 (18.3)	757 (4.00)	NA
Fraction		0.693 (19.6)	NA	NA	NA	NA	NA	NA	NA	NA	NA
Interindividual variability ^a											
ω _{CL_{PL}}	%	NA	NA	37.4 (46.8)	17.8 (39.5)	42.0 (62.5)	73.8 (12.5)	23.9 (15.3)	14.4 (29.8)	31.0 (12.0)	72.5 (38.7)
ω _{Q_{PL_PER1}}	%	NA	NA	NA	28.8 (29.4)	NA	NA	24.3 (28.2)	NA	25.1 (12.1)	NA
ω _{Q_{PL_PER2}}	%	NA	NA	42.5 (42.0)	86.7 (19.3)	NA	NA	NA	NA	76.7 (13.5)	NA
ω _{V_{PL}}	%	NA	NA	40.4 (75.5)	80.6 (17.2)	47.5 (81.4)	75.0 (27.2)	NA	NA	64.1 (32.9)	53.7 (78.8)
ω _{V_{PER1}}	%	51.8 (86.0)	NA	NA	46.0 (15.3)	NA	NA	12.8 (26.6)	NA	NA	NA
ω _{V_{PER2}}	%	NA	NA	NA	NA	NA	NA	NA	NA	NA	NA
Interoccasional variability ^b											
ω _{study1}	%	NA	NA	NA	42.7 (16.2)	NA	NA	NA	NA	NA	NA
ω _{study2}	%	NA	NA	NA	29.7 (30.5)	NA	NA	NA	NA	NA	NA
Residual error ^c											
σ _{plasma proportional}	%	23.7 (35.0)	48.6 (56.1)	15.1 (17.2)	24.6 (8.80)	22.7 (15.6)	13.0 (10.6)	24.5 (7.70)	14.1 (8.60)	31.0 (11.2)	47.2 (49.1)
σ _{plasma additive}	ng/mL	NA	NA	5,400 (42.6)	NA	NA	NA	NA	NA	NA	0.0244 (27.6)

CL_{PL}, clearance from the central compartment; Fraction, percentage of the drug which is reabsorbed by enterohepatic circulation; NA, not applicable; Q_{PL_PER1}, intercompartmental clearance between the central compartment and the peripheral compartment 1; Q_{PL_PER2}, intercompartmental clearance between the central compartment and the peripheral compartment 2; RSE, relative standard error; V_{PL}, distribution volume of the central compartment; V_{PER1}, distribution volume of the peripheral compartment 1; V_{PER2}, distribution volume of the peripheral compartment 2.

^a $\omega_{\theta_{lh}} = \theta_{lh} \times \hat{\omega}_{\theta_{lh}} + \eta_{lh}$, where θ_{lh} represents the parameters of the l th subject and h th study, θ represents the population mean value of the parameter, η_l is the random effect of the l th subject under the assumption of a normal distribution with a mean value of 0 and variance of $\omega_{\theta_{lh}}^2$, and η_{lh} is the random effect of the h th study under the assumption of a normal distribution with a mean value of 0 and variance of $\omega_{\theta_{lh}}^2$.

^bC_{ij} = Y_{IPRED,ij} × (1 + ε_{ij}) or C_{ij} = Y_{IPRED,ij} × (1 + ε_{1,ij}) + ε_{2,ij}, where C_{ij} represents the j th observed concentration of the i th subject, Y_{IPRED,ij} represents the j th individual prediction of the i th subject, and ε_{ij} is the random effect of the j th observed concentration of the i th subject under the assumption of a normal distribution with a mean value of 0 and variance of σ^2 .

Table 3 System-specific parameters of the PBPK model

Description	Parameter	Value	Reference
Volumes	Brain	V_{tot}	1880 μl
	Brain _{ECF}	V_{brainECF}	290 μl
	Brain _{ICF}	V_{brainICF}	1440 μl
	Total lysosome	V_{LYSO}	18 μl
	CSF _{LV}	V_{CSFLV}	50 μl
	CSF _{TFV}	V_{CSFTFV}	50 μl
	CSF _{CM}	V_{CSFCM}	17 μl
	CSF _{SAS}	V_{CSFSAS}	180 μl
	Brain _{MV}	V_{MV}	60 μl
Flows	Cerebral blood flow	Q_{CBF}	1.2 mL/min
	Brain _{ECF} flow	Q_{ECF}	0.0002 mL/min
	CSF flow	Q_{CSF}	0.0022 mL/min
Surface areas	BBB	SA_{BBB}	263 cm^2 ^b
	BCSFB	SA_{BCSFB}	25 cm^2 ^{c,d}
	Total BCM	SA_{BCM}	3000 cm^2
	Total lysosomal membrane	SA_{LYSO}	1440 cm^2
Width	BBB	$\text{Width}_{\text{BBB}}$	0.3–0.5 μm (0.5 was used in the model)

BBB, blood-brain barrier; BCM, brain cell membrane; BCSFB, blood-cerebrospinal barrier; CBF, cerebral blood flow; CM, cisterna magna; CSF, cerebrospinal fluid; ECF, extracellular fluid; ICF, intracellular fluid; LV, lateral ventricle; LYSO, lysosome; MV, microvascular; SA, surface area; SAS, subarachnoid space; TFV, third and fourth ventricle; TOT; total; V, volume.

^aBased on the volume ratio of lysosomes to brain_{ICF} (1:80).¹⁰

^bA total of 99.8% of SA_{BBB} are used for transcellular diffusion, and 0.006% of SA_{BBB} are used for paracellular diffusion.

^cA total of 99.8% of SA_{BCSFB} are used for transcellular diffusion and 0.016% of SA_{BCSFB} are used for paracellular diffusion.

^d SA_{BCSFB1} and SA_{BCSFB2} are assumed to be 12.5 cm^2 and 12.5 cm^2 , respectively.

^eBased on the lysosome number per cell which was calculated using the total lysosomal volume and diameter of each lysosome (0.5–1.0 μm).¹¹

in the brain_{ECF} CSF_{LV}, CSF_{CM}, and total brain tissue with less than twofold prediction error. In comparison, QSPR studies that predict $K_{\text{p,uu,brainECF}}$ of drugs have similar prediction error magnitudes, even though only one parameter was predicted.^{4,5} Therefore, the twofold prediction error is considered to be a good result.

A small underprediction was observed in brain_{ECF} and CSF_{CM} for risperidone, and in brain_{ECF} for morphine at the 4 mg/kg dose. The underprediction of risperidone brain_{ECF} and CSF_{CM} concentrations (**Figure 2**) likely results from difficulties in the plasma PK modeling of risperidone, which leads to propagation of an error in the PBPK model. Risperidone plasma PK data appeared to follow a two-compartment PK model but data were insufficient to describe this two-compartment kinetics. The small underprediction for morphine brain_{ECF} profiles at a dosage of 4 mg/kg might be related to a large interstudy variability for morphine, because the predictions for morphine at the other dosage groups could adequately capture the observations (**Supplementary Figure S1 and Table S1**).

This is the first time that the transcellular and paracellular diffusion clearance at the BBB/BCSFB were addressed separately, by using the information of the intercellular space and the effective pore size. As the contribution of these pathways may depend on the condition of the barriers (i.e., in certain disease conditions the tight junctions may become less tight), therefore, assessment of these system-specific parameters is important. From the electron microscopic cross-section picture of brain capillary,¹² the intercellular space was measured to be 0.03 μm , which is comparable to the 0.02 μm width reported.⁴⁵ Based on the relationship of the pore size and TEER, which were obtained from *in vitro*

studies,¹⁵ we assumed the effective pore size of the BBB and BCSFB to be 0.0011 μm and 0.0028 μm , respectively. The effective pore size derived for the rat BBB (0.0011 μm) is within the range reported in literature (0.0007–0.0018 μm).^{46,47} Therefore, it is reasonable to assume that our estimations for these system-specific parameter values are appropriate. In this study, no compound with sole paracellular transport (such as mannitol) has been used, as no such data were available in literature.

For the PBPK model, the drug-specific parameters were obtained from *in silico* predictions using the compounds' physicochemical properties, except for AF values. The AF values were calculated using $K_{\text{p,uu}}$ values, as obtained from the previously published *in vivo* animal experiments.⁹ It should be noted that $K_{\text{p,uu}}$ values can also be obtained from several published QSPR models using the compound's physicochemical properties.^{3–5}

Unlike previously developed PBPK models for the CNS,² our PBPK model contains a number of key relevant physiological processes and compartments.

We discriminated between paracellular and transcellular diffusion processes. The relative impact of the paracellular diffusion on Q_{BBB} or Q_{BCSFB} for each compound varied from around 100% (methotrexate) to 1.3% (quinidine). For hydrophilic compounds, Q_{BBB} and Q_{BCSFB} were impacted most by paracellular diffusion, whereas transcellular diffusion largely determined the Q_{BBB} and Q_{BCSFB} of lipophilic compounds. The separation of the two processes is expected to be meaningful for the prediction of the CNS drug concentrations in disease conditions, because pathophysiological conditions may differently affect paracellular and transcellular diffusion.

Table 4 Drug-specific parameters of the PBPK model

		Acetaminophen	Atenolol	Methotrexate	Morphine	Paliperidone	Phenytoin	Quinidine	Raclopride	Remoxipride	Risperidone
Drug specific parameters											
Transmembrane permeability	cm/min	1.1*10 ⁻⁴	5.7*10 ⁻⁵	6.1*10 ⁻⁷	2.5*10 ⁻⁴	0.0018	0.0077	0.058	6.6*10 ⁻⁴	0.0035	0.0082
Aqueous diffusivity coefficient (paracellular diffusion)	cm ² /min	4.6*10 ⁻⁴	3.5*10 ⁻⁴	2.8*10 ⁻⁴	3.4*10 ⁻⁴	2.8*10 ⁻⁴	3.6*10 ⁻⁴	3.2*10 ⁻⁴	3.1*10 ⁻⁴	3.0*10 ⁻⁴	2.9*10 ⁻⁴
AF											
AFin1		1.0	1.0	1.0	1.0	1.0	1.0	1.2	1.0	1.0	1.0
AFin2		1.0	1.0	1.0	1.0	1.0	1.0	1.4	1.0	1.0	1.0
AFin3		1.0	1.0	1.0	1.0	1.0	1.0	1.4	1.0	1.0	1.0
AFout1		12	40	4.6*10 ⁻⁴	11 ^a , 20 ^b	3.0	4.2	1.0	1.4	1.7	1.3
AFout2		29	82	4.7*10 ⁻⁵	20 ^a , 38 ^b	3.7	7.6	1.0	1.1	1.7	1.3
AFout3		32	110	1.0*10 ⁻⁶	26 ^a , 49 ^b	4.7	7.7	1.0	1.9	2.1	1.5
Partitioning coefficient between compartments											
Kp,uu,brain _{ECF}		0.51	0.37	0.018	0.38 ^a , 0.23 ^b	0.50	0.26	1.5	1.1	0.80	0.97
Kp,uu,CSF _{LV}		0.51	0.37	0.0066	0.38 ^a , 0.23 ^b	0.50	0.26	1.5	1.1	0.80	0.97
Kp,uu,CSF _{CM}		0.51	0.37	0.0024	0.38 ^a , 0.23 ^b	0.50	0.26	1.5	1.1	0.80	0.97
Kp		1.0	0.94	NA	1.3	1.3	2.3	13	11	5.5	2.1
Free fraction											
fu,p		0.81	0.91	0.45	0.83	0.080	0.090	0.14	0.070	0.74	0.070
fu,b		0.80	0.90	NA	0.76	0.065 ^d	0.080	0.090	0.13	0.57 ^c	0.065
Physicochemical properties											
Molecular weight		151	266	454	285	426	252	324	347	371	410
log P		0.5	0.2	-1.9	0.9	1.8	2.5	3.4	1.3	2.1	2.5
pKa (acid)		9.5	14.1	3.4	10.3	13.7	9.5	13.9	5.9	13.1	
pKa (base)		-4.4	9.7	2.8	9.1	8.8	-9.0	9.1	9.0	8.4	8.8
Charge class		Neutral	Base	Acid	Base	Base	Neutral	Base	Zwitterion	Base	Base

AF, asymmetry factor; Kp,uu,brain_{ECF}, unbound brain extracellular fluid-to-plasma concentration ratio; Kp,uu,CSF_{LV}, unbound CSF_{LV}-to-plasma concentration ratio; Kp,uu,CSF_{CM}, unbound CSF_{CM}-to-plasma concentration ratio; Kp, total brain-to-plasma concentration ratio; fu,p, free fraction in plasma; fu,b, free fraction in brain.

^aAFin1-3 and AFout1-3 were calculated from Kp,uu,brain_{ECF}, Kp,uu,CSF_{LV}, and Kp,uu,CSF_{CM}, respectively.

^b40 mg/kg.

^cCalculated from Vu,brain, and Kp,uu,cell.

^dAssumed to be the same as risperidone.

Table 5 Combined parameters of system-specific and drug-specific parameters in the PBPK model

Parameter	Unit	Acetaminophen	Atenolol	Methotrexate	Morphine	Paliperidone	Phenytoin	Quinidine	Raclopride	Remoxipride	Risperidone
Q_{BBB_in}	mL/min	0.16	0.12	0.087	0.14	0.33	1.1	9.1	0.18	0.55	1.2
Q_{BBB_out}	mL/min	0.31	0.33	4.8	$0.38^a, 0.62^b$	0.65	4.4	5.1	0.18	0.69	1.2
Q_{BBB}	mL/min	0.014	0.0075	8.0×10^{-5}	0.033	0.24	1.0	7.6	0.086	0.46	1.1
Q_{BBB}	mL/min	0.14	0.11	0.087	0.11	0.090	0.11	0.10	0.099	0.096	0.091
PHF1		1.0	0.80	1.3	0.80	0.80	1.0	0.80	0.80	0.81	0.80
Q_{BCSFB1_in}	mL/min	0.019	0.014	0.011	0.015	0.023	0.063	0.52	0.020	0.034	0.063
Q_{BCSFB1_out}	mL/min	0.038	0.034	2.2	$0.036^a, 0.059^b$	0.042	0.38	0.21	0.013	0.040	0.063
Q_{BCSFB1}	mL/min	6.8×10^{-4}	3.6×10^{-4}	3.8×10^{-6}	0.0016	0.011	0.048	0.36	0.0041	0.022	0.051
Q_{BCSFB1}	mL/min	0.018	0.014	0.011	0.014	0.011	0.014	0.013	0.012	0.012	0.012
PHF2		1.0	0.80	1.3	0.80	0.80	1.0	0.80	0.80	0.81	0.80
Q_{BCSFB2_in}	mL/min	0.019	0.014	0.011	0.015	0.023	0.063	0.52	0.017	0.034	0.063
Q_{BCSFB2_out}	mL/min	0.040	0.042	4.9	$0.044^a, 0.073^b$	0.052	0.38	0.21	0.016	0.047	0.073
Q_{BCSFB2}	mL/min	6.8×10^{-4}	3.6×10^{-4}	3.8×10^{-6}	0.0016	0.011	0.048	0.36	0.0041	0.022	0.051
Q_{BCSFB2}	mL/min	0.018	0.014	0.011	0.014	0.011	0.014	0.013	0.012	0.012	0.012
PHF3		1.0	0.80	1.3	0.80	0.80	1.0	0.80	0.80	0.81	0.80
Q_{BCM_in}	mL/min	0.33	0.14	0.0023	0.61	4.4	23	140	1.6	8.4	20
Q_{BCM_out}	mL/min	0.33	0.068	0.0046	0.31	2.2	23	70	0.80	4.4	10
PHF4		1.0	0.80	1.3	0.80	0.80	1.0	0.80	0.80	0.81	0.80
PHF5		1.0	0.40	2.5	0.40	0.41	1.0	0.40	0.40	0.42	0.41
Q_{LYSO_in}	mL/min	0.16	0.033	0.0022	0.15	1.1	11	33	0.38	2.1	4.8
Q_{LYSO_out}	mL/min	0.16	0.00033	0.21	0.0015	0.011	11	0.34	0.0039	0.022	0.049
PHF6		1.0	0.40	2.5	0.40	0.41	1.0	0.40	0.40	0.42	0.41
PHF7		1.0	0.0040	250	0.0041	0.0041	1.0	0.0041	0.0041	0.0044	0.0041
BF		1.1	0.92	NA	$1.8^a, 3.9^b$	0.91	8.2	7.2	8.5	5.3	0.49

BBB, blood-brain barrier; BCM, brain cell membrane; BCSFB, blood-cerebrospinal fluid barrier; BF, binding factor; LYSO, lysosome; PHF, pH-dependent factor; Q_{BBB} , passive diffusion clearance at the BBB; Q_{BCSFB1} , transcellular diffusion clearance at the BCSFB1; Q_{BCSFB2} , transcellular diffusion clearance at the BCSFB2; Q_{BCM_in} , transmembrane permeability at the BCM; Q_{BCM_out} , transmembrane permeability at the BCM; Q_{LYSO_in} , transmembrane permeability at the LYSO; Q_{LYSO_out} , transmembrane permeability at the LYSO; Q_{BCSFB1} , transcellular diffusion clearance at the BCSFB1; Q_{BCSFB2} , transcellular diffusion clearance at the BCSFB2; Q_{BCM} , passive diffusion clearance at the lysosomal membrane; Q_{BBB} , passive diffusion clearance at the brain cell membrane; Q_{LYSO} , passive diffusion clearance at the lysosomal membrane.

$Q_{BBB_in} = Q_{BBB} + Q_{BBB} \cdot A_{Fin1}$, $Q_{BBB_out} = (Q_{BBB} + Q_{BBB} \cdot A_{Fout1}) \cdot PHF1$, $Q_{BBB} = (\text{aqueous diffusivity coefficient} / \text{width}_{BBB}) \cdot SA_{BBB}$, $Q_{BBB} = 1/2 \cdot \text{transmembrane permeability} \cdot SA_{BBB}$

$Q_{BCSFB1_in} = Q_{BCSFB1} + Q_{BCSFB1_out} = (Q_{BCSFB1} + Q_{BCSFB1} \cdot A_{Fin2}) \cdot PHF2$, $Q_{BCSFB1} = (\text{aqueous diffusivity coefficient} / \text{width}_{BCSFB1}) \cdot SA_{BCSFB1}$, $Q_{BCSFB1} = 1/2 \cdot \text{transmembrane permeability} \cdot SA_{BCSFB1}$

$Q_{BCSFB2_in} = Q_{BCSFB2} + Q_{BCSFB2_out} = (Q_{BCSFB2} + Q_{BCSFB2} \cdot A_{Fout3}) \cdot PHF3$, $Q_{BCSFB2} = (\text{aqueous diffusivity coefficient} / \text{width}_{BCSFB2}) \cdot SA_{BCSFB2}$, $Q_{BCSFB2} = 1/2 \cdot \text{transmembrane permeability} \cdot SA_{BCSFB2}$

$Q_{BCM_in} = \text{Transmembrane permeability} \cdot SA_{BCM} \cdot PHF4$, $Q_{BCM_out} = \text{transmembrane permeability} \cdot SA_{BCM} \cdot PHF5$, $Q_{LYSO_in} = \text{transmembrane permeability} \cdot SA_{LYSO} \cdot PHF6$, $Q_{LYSO_out} = \text{transmembrane permeability} \cdot SA_{LYSO} \cdot PHF7$.

PHF1, PHF2, PHF3, PHF4, PHF5, PHF6, and PHF7 were calculated from pKa of each compound and pH of each compartment, respectively.

BF was calculated from Kp of each compound.

^a4 mg/kg.

^b10, 40 mg/kg.

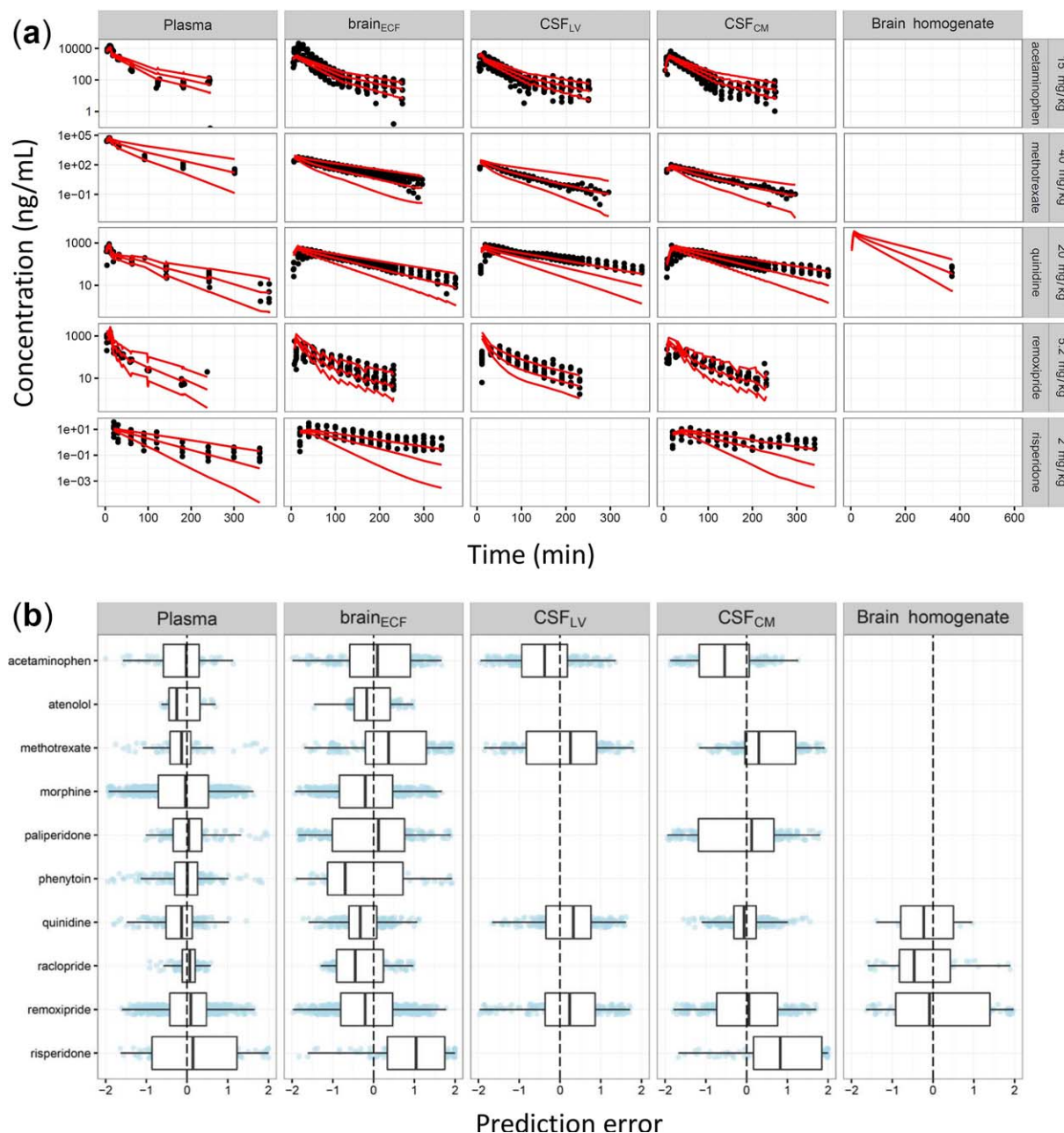


Figure 2 Prediction accuracy of the physiologically based pharmacokinetic (PBPK) model. The plots were stratified by the central nervous system (CNS) compartments (panels). (a) Selected individual observed drug concentrations (dots) and 95% prediction interval (red lines). (b) Box-whisker plots for the prediction errors (PEs) across all 10 drugs evaluated. Blue dots are PEs for each observation.

We also demonstrated the relevance of considering CBF-limited kinetics on the drug transfer at the BBB. For the lipophilic compounds, Q_{BBB_in} and Q_{BBB_out} are higher than Q_{CBF} indicating that the drug transfer clearance on the BBB is largely determined by Q_{CBF} .

The importance of the separation between brain_{ECF} and brain_{ICF} compartments was shown. The Q_{BCM_in} and Q_{BCM_out} were either higher or lower than Q_{BBB_in} and Q_{BBB_out} , depending on the molecular weight, the log P, and the pKa of the compound, which led to differences in drug distribution into brain_{ICF} from brain_{MV}.

We identified differences in methotrexate drug concentration in CSF_{LV} and CSF_{CM}.²³ Therefore, it is expected that the expression level (function) of some of the active transporters may be different between the BCSFB around CSF_{LV} and CSF_{TFV}. Methotrexate is known to be a substrate of various transporters, such as RFC1, MRP, BCRP, OATP, and OAT transporters,²³ even though there is no detailed information about their exact location. Therefore, we incorporated this in our model by including Q_{BCSFB1} and Q_{BCSFB2} to describe transport for methotrexate.

All of the parameters for our CNS PBPK model can be derived from either literature or *in silico* predictions. Therefore, the model can be used to assess newly developed CNS drugs without *in vivo* data and contributes to the “refinement, reduction, and replacement” of animals in drug research. Although the reported values of the system-specific parameters for humans are sparse and variable,² theoretically, the model can be scaled to humans by replacing the system-specific parameters to predict target-site concentrations in the human brain, representing an important tool for translational development of new CNS drugs.

Acknowledgments. This research article was prepared within the framework of project number D2–501 of the former Dutch Top Institute Pharma, currently Lygature (Leiden, The Netherlands; www.lygature.org). J.G.C.H. received funding from the European Union Marie Curie programme (Project ID 661588).

Conflict of Interest. The authors have no conflicts of interest that are directly relevant to the contents of this research article.

Author Contributions. E.C.M.L., Y.Y., P.A.V., D.R., J.H.P., A.V., W.K., M.W.B., M.D., and J.G.C.H. wrote the manuscript; E.C.M.L. designed the research; E.C.M.L., Y.Y., P.A.V., and J.G.C.H. performed the research; D.J.B., R.H., and Y.C.W. analyzed the data.

1. Kola, I. & Landis, J. Can the pharmaceutical industry reduce attrition rates? *Nat. Rev. Drug Discov.* **3**, 711–715 (2004).
2. Yamamoto, Y., Danhof, M. & de Lange, E.C.M. Microdialysis: the key to physiologically based model prediction of human CNS target site concentrations. *AAPS J.* **19**, 891–909 (2017).
3. Fridén, M. *et al.* Structure-brain exposure relationships in rat and human using a novel data set of unbound drug concentrations in brain interstitial and cerebrospinal fluids. *J. Med. Chem.* **52**, 6233–6243 (2009).
4. Loryan, I. *et al.* Molecular properties determining unbound intracellular and extracellular brain exposure of CNS drug candidates. *Mol. Pharm.* **12**, 520–532 (2015).
5. Chen, H., Winiwarter, S., Fridén, M., Antonsson, M. & Engkvist, O. In silico prediction of unbound brain-to-plasma concentration ratio using machine learning algorithms. *J. Mol. Graph. Model.* **29**, 985–995 (2011).
6. Jones, H. & Rowland-Yeo, K. Basic concepts in physiologically based pharmacokinetic modeling in drug discovery and development. *CPT Pharmacometrics Syst. Pharmacol.* **2**, e63 (2013).
7. Engelhardt, B. & Sorokin, L. The blood-brain and the blood-cerebrospinal fluid barriers: function and dysfunction. *Semin. Immunopathol.* **31**, 497–511 (2009).
8. Nguyen, T.H. *et al.* Model evaluation of continuous data pharmacometric models: metrics and graphics. *CPT Pharmacometrics Syst. Pharmacol.* **6**, 87–109 (2017).
9. Yamamoto, Y. *et al.* A generic multi-compartmental CNS distribution model structure for 9 drugs allows prediction of human brain target site concentrations. *Pharm. Res.* **34**, 333–351 (2017).
10. Nicholson, C. & Syková, E. Extracellular space structure revealed by diffusion analysis. *Trends Neurosci.* **21**, 207–215 (1998).
11. Hardin, J., Bertoni, G.P. & Kleinsmith, L.J. *Becker's World of the Cell, Books a la Carte Edition (8th Edition)*. (Pearson Education, San Francisco, CA, 2011).
12. Weiss, N., Miller, F., Cazaubon, S. & Couraud, P.O. The blood-brain barrier in brain homeostasis and neurological diseases. *Biochim. Biophys. Acta* **1788**, 842–857 (2009).
13. Crone, C. & Olesen, S.P. Electrical resistance of brain microvascular endothelium. *Brain Res.* **241**, 49–55 (1982).
14. Olesen, S.P. & Crone, C. Electrical resistance of muscle capillary endothelium. *Biophys. J.* **42**, 31–41 (1983).
15. Adson, A. *et al.* Quantitative approaches to delineate paracellular diffusion in cultured epithelial cell monolayers. *J. Pharm. Sci.* **83**, 1529–1536 (1994).
16. Avdeef, A., Nielsen, P.E. & Tsinman, O. PAMPA – a drug absorption in vitro model 11. Matching the in vivo unstirred water layer thickness by individual-well stirring in microtitre plates. *Eur. J. Pharm. Sci.* **22**, 365–374 (2004).
17. Grumetto, L., Russo, G. & Barbato, F. Immobilized artificial membrane HPLC derived parameters vs PAMPA-BBB data in estimating in situ measured blood-brain barrier permeation of drugs. *Mol. Pharm.* **13**, 2808–2816 (2016).

18. Fridén, M. *et al.* Measurement of unbound drug exposure in brain: modeling of pH partitioning explains diverging results between the brain slice and brain homogenate methods. *Drug Metab. Dispos.* **39**, 353–362 (2011).
19. Henderson, L.J. Concerning the relationship between the strength of acids and their capacity to preserve neutrality. *Am. J. Physiol.* **21**, 173–179 (1908).
20. Henderson, L.J. The theory of neutrality regulation in the animal organism. *Am. J. Physiol.* **21**, 427–448 (1908).
21. Berezhkovskiy, L.M. Volume of distribution at steady state for a linear pharmacokinetic system with peripheral elimination. *J. Pharm. Sci.* **93**, 1628–1640 (2004).
22. Poulin, P. & Theil, F.P. Prediction of pharmacokinetics prior to in vivo studies. II. Generic physiologically based pharmacokinetic models of drug disposition. *J. Pharm. Sci.* **91**, 1358–1370 (2002).
23. Westerhout, J., van den Berg, D.J., Hartman, R., Danhof, M. & de Lange, E.C. Prediction of methotrexate CNS distribution in different species – Influence of disease conditions. *Eur. J. Pharm. Sci.* **57**, 11–24 (2014).
24. Westerhout, J., Ploeger, B., Smeets, J., Danhof, M. & de Lange, E.C. Physiologically based pharmacokinetic modeling to investigate regional brain distribution kinetics in rats. *AAPS J.* **14**, 543–553 (2012).
25. de Lange, E.C., Danhof, M., de Boer, A.G. & Breimer, D.D. Critical factors of intracerebral microdialysis as a technique to determine the pharmacokinetics of drugs in rat brain. *Brain Res.* **666**, 1–8 (1994).
26. Groenendaal, D., Freijer, J., de Mik, D., Bouw, M.R., Danhof, M. & de Lange, E.C. Population pharmacokinetic modelling of non-linear brain distribution of morphine: influence of active saturable influx and P-glycoprotein mediated efflux. *Br. J. Pharmacol.* **151**, 701–712 (2007).
27. Bouw, M.R., Gårdmark, M. & Hammarlund-Udenaes, M. Pharmacokinetic-pharmacodynamic modelling of morphine transport across the blood-brain barrier as a cause of the antinociceptive effect delay in rats—a microdialysis study. *Pharm. Res.* **17**, 1220–1227 (2000).
28. Westerhout, J., Smeets, J., Danhof, M. & de Lange, E.C. The impact of P-gp functionality on non-steady state relationships between CSF and brain extracellular fluid. *J. Pharmacokinet. Pharmacodyn.* **40**, 327–342 (2013).
29. Stevens, J., Ploeger, B.A., van der Graaf, P.H., Danhof, M. & de Lange, E.C. Systemic and direct nose-to-brain transport pharmacokinetic model for remoxipride after intravenous and intranasal administration. *Drug Metab. Dispos.* **39**, 2275–2282 (2011).
30. Kawakami, J., Yamamoto, K., Sawada, Y. & Iga, T. Prediction of brain delivery of ofloxacin, a new quinolone, in the human from animal data. *J. Pharmacokinet. Biopharm.* **22**, 207–227 (1994).
31. Cserr, H.F., Cooper, D.N., Suri, P.K. & Patlak, C.S. Efflux of radiolabeled polyethylene glycols and albumin from rat brain. *Am. J. Physiol.* **240**, F319–F328 (1981).
32. Thorne, R.G., Hrabětová, S. & Nicholson, C. Diffusion of epidermal growth factor in rat brain extracellular space measured by integrative optical imaging. *J. Neurophysiol.* **92**, 3471–3481 (2004).
33. Condon, P. *et al.* Use of magnetic resonance imaging to measure intracranial cerebrospinal fluid volume. *Lancet*. **1**, 1355–1357 (1986).
34. Kohn, M.I. *et al.* Analysis of brain and cerebrospinal fluid volumes with MR imaging. Part I. Methods, reliability, and validation. *Radiology* **178**, 115–122 (1991).
35. Robertson, E.G. Developmental defects of the cisterna magna and dura mater. *J. Neurol. Neurosurg. Psychiatry* **12**, 39–51 (1949).
36. Adam, R. & Greenberg, J.O. The mega cisterna magna. *J. Neurosurg.* **48**, 190–192 (1978).
37. Bass, N.H. & Lundborg, P. Postnatal development of bulk flow in the cerebrospinal fluid system of the albino rat: clearance of carboxyl-(14 C)inulin after intrathecal infusion. *Brain Res.* **52**, 323–332 (1973).
38. Liu, X. *et al.* Use of a physiologically based pharmacokinetic model to study the time to reach brain equilibrium: an experimental analysis of the role of blood-brain barrier permeability, plasma protein binding, and brain tissue binding. *J. Pharmacol. Exp. Ther.* **313**, 1254–1262 (2005).
39. Neuwelt, E. *et al.* Strategies to advance translational research into brain barriers. *Lancet Neurol.* **7**, 84–96 (2008).
40. Patabendige, A., Skinner, R.A. & Abbott, N.J. Establishment of a simplified in vitro porcine blood-brain barrier model with high transendothelial electrical resistance. *Brain Res.* **1521**, 1–15 (2013).
41. Strazielle, N. & Gherzi-Egea, J.F. Choroid plexus in the central nervous system: biology and pathophysiology. *J. Neuropathol. Exp. Neurol.* **59**, 561–574 (2000).
42. Trapa, P.E., Belova, E., Liras, J.L., Scott, D.O. & Steyn, S.J. Insights from an integrated physiologically based pharmacokinetic model for brain penetration. *J. Pharm. Sci.* **105**, 965–971 (2016).
43. Cornford, E.M. & Hyman, S. Localization of brain endothelial luminal and abluminal transporters with immunogold electron microscopy. *NeuroRx* **2**, 27–43 (2005).
44. Sasaki, Y. & Wagner, H.N. Jr. Measurement of the distribution of cardiac output in unanesthetized rats. *J. Appl. Physiol.* **30**, 879–884 (1971).
45. Farquhar, M.G. & Palade, G.E. Junctional complexes in various epithelia. *J. Cell. Biol.* **17**, 375–412 (1963).
46. Crone, C. Lack of selectivity to small ions in paracellular pathways in cerebral and muscle capillaries of the frog. *J. Physiol.* **353**, 317–337 (1984).
47. Zhang, T.T., Li, W., Meng, G., Wang, P. & Liao, W. Strategies for transporting nanoparticles across the blood-brain barrier. *Biomater. Sci.* **4**, 219–229 (2016).

© 2017 The Authors CPT: Pharmacometrics & Systems Pharmacology published by Wiley Periodicals, Inc. on behalf of American Society for Clinical Pharmacology and Therapeutics. This is an open access article under the terms of the Creative Commons Attribution-

NonCommercial-NoDerivs License, which permits use and distribution in any medium, provided the original work is properly cited, the use is non-commercial and no modifications or adaptations are made.

Supplementary information accompanies this paper on the *CPT: Pharmacometrics & Systems Pharmacology* website (<http://psp-journal.com>)